Nanoscale

Accepted Manuscript

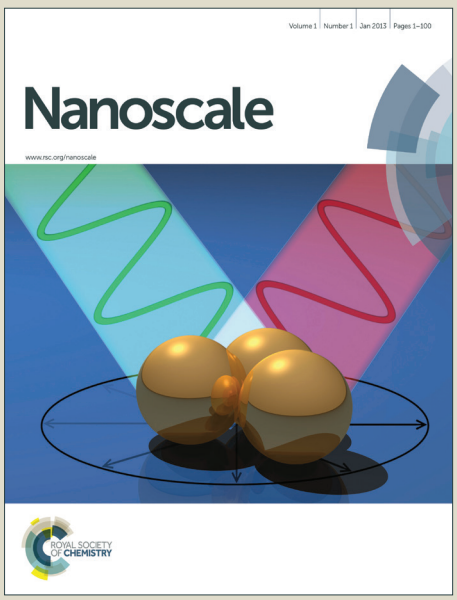

ROYAL SOCIETY OF CHEMISTRY

www.rsc.org/nanoscale

Cite this: DOI: 10.1039/c0xx00000x

www.rsc.org/xxxxxx

COMMUNICATION

Synthesis of PEGylated low generation dendrimer-entrapped gold nanoparticles for CT imaging applications†

Hui Liu,[‡a,b] Han Wang,[‡c] Yanhong Xu,[c] Mingwu Shen,[b] Jinglong Zhao,[c] Guixiang Zhang*[c] and Xiangyang Shi*[a,b,d]

Received (in XXX, XXX) Xth XXXXXXXXX 20XX, Accepted Xth XXXXXXXXX 20XX
DOI: 10.1039/b000000x

Dendrimer-entrapped gold nanoparticles (Au DENPs) can be formed using low-generation dendrimers pre-modified by polyethylene glycol (PEG). The formed PEGylated Au DENPs with desirable stability, cytocompatibility, and X-ray attenuation property enable efficient computed tomography imaging of the heart and tumor model of mice.

Computed tomography (CT) has been considered to be one of the most powerful molecular imaging techniques due to its high density resolution, deep tissue penetration, rapid scan speed, and cost effectiveness.[1, 2] For effective and specific CT imaging, contrast agents are generally required.[3-6] The conventionally used small molecular iodinated CT contrast agents (e.g., Omnipaque)[7] suffer severe drawbacks of short blood circulation time, lack of tissue specificity, and renal toxicity at a relatively high concentration, quite limiting their CT imaging applications.[8, 9] It is important to develop new contrast agents to overcome the above drawbacks.

Recent advances in nanotechnology have enabled the generation of various inorganic nanoparticulate contrast agents for CT imaging applications.[2, 10, 11] In particular, Bi_2S_3 nanoparticles (NPs),[12-14] Yb-based NPs,[5, 15] and gold NPs (AuNPs)[16-21] have been developed for various CT imaging applications. These nanosized CT contrast agents share the common advantages, such as prolonged blood circulation time due to the nanoscale size and high X-ray attenuation coefficient due to the high atomic number of the radiodense element. Among the developed inorganic NP-based CT contrast agents, AuNPs have been quite attractive because of the advantages of easy synthesis, good stability, and good biocompatibility after proper surface functionalization.[17, 18, 22-24]

To form stable and biocompatible AuNPs, dendrimers, especially poly(amidoamine) (PAMAM) dendrimers have been used as excellent templates or stabilizers to form dendrimer-entrapped AuNPs (Au DENPs) or dendrimer-stabilized AuNPs (Au DSNPs).[25-31] Dendrimers are a class of highly branched, monodispersed, synthetic macromolecules with well-defined structure, composition, and geometry.[32] With the unique structural features of dendrimers, Au DENPs having a structure of one AuNP entrapped within each dendrimer molecule can be formed using dendrimers as templates *via* a fast reducing reaction and the formed Au core NPs are usually smaller than 5 nm.[27, 29, 33-35] Alternatively, Au DSNPs with Au core size usually larger than 5 nm can be prepared using dendrimers as stabilizers under weak reducing conditions. In this case, Au DSNPs denote to a structure of one AuNP surrounded with multiple dendrimers.[24, 36-38] Our previous work has shown that several kinds of Au DENPs[7, 18, 27, 39] and Au DSNPs[23, 24, 38, 40] can be formed and used as contrast agents for CT imaging applications. To render the particles with desired biocompatibility, acetylation of the dendrimer terminal amines after the formation of the particles is usually performed. Additionally, polyethylene glycol (PEG) has also been modified onto the dendrimer surface for subsequent formation of Au DENPs for CT imaging of cancer cells *in vitro* and *in vivo*,[41, 42] since PEGylation modification of particle surfaces is proven to afford the particles with good stability and desirable biocompatibility.[22, 43-45] Importantly, our studies demonstrate that the PEGylation modification of generation 5 (G5) dendrimer surface enables enlarged dendrimer periphery that can be used to load more Au element within the dendrimer interior.[33, 34, 41, 42] In most of these studies, high-generation dendrimers (e.g., G5) have been used to generate Au DENPs or Au DSNPs for CT imaging applications. Recently, we have shown that stable and biocompatible Au DSNPs can be successfully formed using generation 2 (G2) dendrimers with a size of 2.9 nm as stabilizers *via* a hydrothermal approach for CT imaging applications.[23, 24] These prior successes lead us to hypothesize that PEGylated low-generation dendrimers with enlarged periphery may be used as templates to form Au DENPs, thereby providing a facile strategy to avoid using expensive high-generation dendrimers. This is of significance for their further biomedical applications.

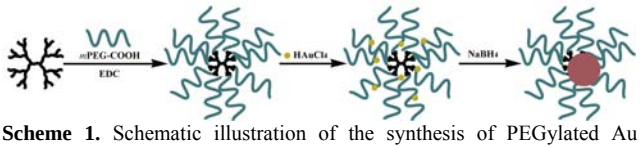

Scheme 1. Schematic illustration of the synthesis of PEGylated Au DENPs using G2 dendrimers.

In this present study, amine-terminated G2 PAMAM dendrimers ($G2.NH_2$) were firstly modified with PEG chains and then employed as templates to form Au DENPs *via* a chemical reduction protocol (Scheme 1). The formed PEGylated Au DENPs were characterized *via* different techniques. 3-(4,5-Dimethyl-thiazol-2-yl)-2,5-diphenyltetrazolium bromide (MTT)

cell viability assay was used to evaluate the cytotoxicity of the particles. Finally, the PEGylated Au DENPs were used for CT imaging of organs and a tumor model of mice after intravenous injection of the particles. To our knowledge, this is the first report related to the formation of PEGylated Au DENPs using low-generation dendrimers for CT imaging applications.

Due to the relatively open structure and small size, amine-terminated low generation PAMAM dendrimers are unable to entrap AuNPs within the dendrimer interior even under strong reducing conditions, and in most of the cases, Au DSNPs are formed.[36, 46] With the advantages of PEGylation that have been proven to be capable to enlarge the dendrimer periphery for more Au loading within the dendrimer interiors, to improve the biocompatibility of the particles, and to prolong the blood circulation time of the particles in our previous work,[33, 34, 41, 42] we attempted to modify the periphery of G2.NH_2 dendrimers *via* PEGylation for possible formation of Au DENPs.

G2.NH_2 dendrimers were firstly modified with *m*PEG-COOH *via* an 1-ethyl-3-(3-dimethylaminopropyl) carbodiimide hydrochloride (EDC) coupling chemistry (Scheme 1). The formed G2-*m*PEG was characterized by ^{1}H NMR (Figure S1a, ESI†). The appearance of the methylene proton signal associated with *m*PEG at 3.5 ppm clearly indicates the formation of G2-*m*PEG conjugate. By NMR integration of the protons associated with *m*PEG and G2 dendrimer, the number of *m*PEG moieties attached onto each G2 dendrimer was estimated to be 10.0.

The formed G2-*m*PEG conjugates were then employed as templates to form Au DENPs through $NaBH_4$ reduction chemistry. Under the selected Au salt/dendrimer molar ratio of 8:1, stable AuNPs with a typical wine red color were formed. It should be noted that at an Au salt/dendrimer molar ratio of more than 8:1, a portion of the particles precipitate, suggesting the instability of the particles. The formation of Au DENPs does not seem to appreciably alter the ^{1}H NMR spectrum of the G2-*m*PEG dendrimers (Figure S1b, ESI†). Zeta-potential measurements show that the surface potential of G2.NH_2 dendrimers decreases from 8.26 to 4.65 mV after modification of *m*PEG, likely due to the expected successful coupling reaction. Further formation of Au DENPs does not seem to significantly alter the surface potential of the particles (3.61 mV) when compared to the G2-*m*PEG dendrimers (Table S1, ESI†). Unlike the formation of PEGylated Au DENPs using G5 dendrimers partially modified with PEG as templates for biomedical imaging applications that requires an additional acetylation step to neutralize the remaining dendrimer terminal amines,[41] it seems that the formed PEGylated Au DENPs with a close to neutral surface potential using G2 dendrimers do not need such an additional acetylation step. This is likely due to the fact that a significant stealth effect of PEG can be achieved by covering 10 amine groups of each G2 dendrimer.

UV-vis spectrometry and TEM were used to characterize the formed {$(Au^0)_8$-G2-*m*PEG} DENPs (Figure 1 and Figure S2, ESI†). An apparent surface plasmon resonance (SPR) band at around 527 nm indicates the formation of AuNPs with a wine red solution color (Figure 1a and inset). TEM data reveal that the formed AuNPs have a spherical shape and a relatively uniform size distribution with a mean diameter of 2.8±0.6 nm (Figure 1b and inset). The hydrodynamic sizes of G2.NH_2, G2-*m*PEG, and PEGylated Au DENPs were measured by DLS (Table S1, ESI†). It can be seen that G2.NH_2 dendrimers have a hydrodynamic size of 542.15 nm with a polydispersity index (PDI) of 0.60. After *m*PEG modification, the size of the dendrimers increases to 820.25 nm with a PDI of 1.00. Further formation of Au DENPs leads to a decreased hydrodynamic size of 276.10 nm with a smaller PDI of 0.78. Our results suggest that PEGylation of G2 dendrimers is able to enlarge the dendrimer periphery to have a bigger hydrodynamic size, while the entrapment of AuNPs within the PEGylated G2 dendrimers seems to appreciably change the aggregation behavior of the particles. It is interesting to note that the measured hydrodynamic size of the Au DENPs is much larger than that measured by TEM. This is likely due to the fact that DLS measures the size of large aggregates or clusters of particles in aqueous solution that may consist of many DENPs, while TEM just measures single metal Au core NPs, in agreement with our previous results.[23, 24] Although the Au DENPs composed of both Au core NPs and the dendrimer templates display certain degree of aggregation in aqueous solution as confirmed by DLS measurements, the Au core particles themselves do not aggregate due to the dendrimer entrapment and protection as confirmed by TEM data. The aggregation state of Au DENPs in a dry state may be partly reflected from the TEM images (Figure 1b and Figure S2, ESI†), where some irregular clustered Au core NPs can be seen. In addition, based on the estimated radius of gyration of G2-PEG dendrimers (2.5 nm) as simulated by well-tempered metadynamics,[47] the formed PEGylated G2 dendrimers in our work are proposed to be able to entrap AuNPs with a mean diameter of 2.8 nm inside the dendrimer interiors. In this case, the scenario of Au DSNPs is unlikely possible.

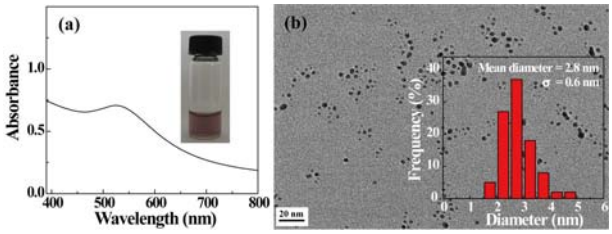

Figure 1. UV-vis spectrum (a) and TEM image (b) of the synthesized PEGylated Au DENPs. Inset of (a) and (b) shows the water solution and size distribution histogram of the particles, respectively.

The crystalline structure of the {$(Au^0)_8$-G2-*m*PEG} DENPs was characterized by both high-resolution TEM and selected area electron diffraction (SAED). Lattices of the PEGylated Au DENPs can be clearly observed in a typical high-resolution TEM image (Figure S3a, ESI†). In addition, the (111), (200), (220), and (311) rings shown in a typical SAED pattern of the Au DENPs (Figure S3b, ESI†) clearly indicate the face-centered-cubic structure of Au crystals.

Stability of the PEGylated Au DENPs is crucial for them to be used for biomedical applications. Since the aggregation state of the AuNPs can be directly reflected by changes of their SPR band,[24, 40] we used UV-vis spectrometry to assess the stability of the {$(Au^0)_8$-G2-*m*PEG} DENPs (Figure S4, ESI†). Figure S4a shows the UV-vis spectra of {$(Au^0)_8$-G2-*m*PEG} DENPs dispersed in water with different pHs (pH = 5, 6, 7, and 8, respectively) at room temperature (25 °C). It can be seen that the absorption features, especially the SPR peak position of the NPs does not have an appreciable change in the pH range of 5-8,

suggesting that the PEGylated Au DENPs show similar aggregation state in the studied pH range. Similarly, no significant SPR peak shifting or broadening occurs when the particles are exposed to water at the temperatures of 4, 25, 37, and 50 °C, respectively (Figure S4b, ESI†), suggesting that the aggregation state of $\{(Au^0)_8$-G2-*m*PEG$\}$ DENPs does not change appreciably at the studied temperatures.

Furthermore, the colloidal stability of the $\{(Au^0)_8$-G2-mPEG$\}$ DENPs was further assessed by dispersing the particles in water, phosphate buffered saline (PBS), and cell culture medium, respectively (Figure S4c, ESI†). It can be found that the particles do not precipitate after at least one month's storage at room temperature. Taken together, the formed $\{(Au^0)_8$-G2-*m*PEG$\}$ DENPs are not only stable at the studied pH and temperature conditions, but also stable in different aqueous media, which is important for their further biomedical applications.

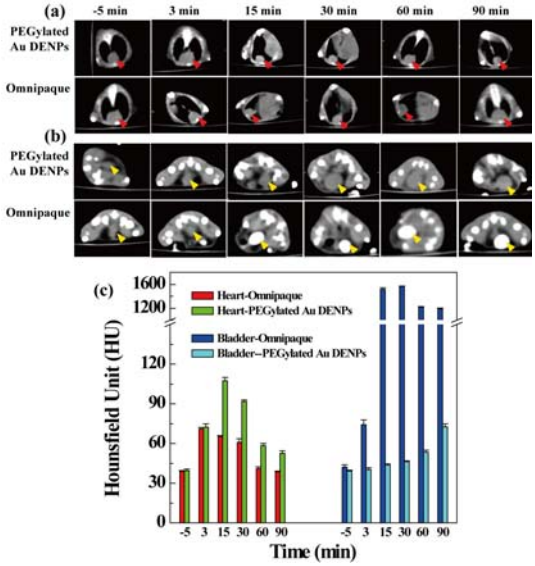

Figure 2. CT images of mouse heart (a) and bladder (b) before and after intravenous injection of PEGylated Au DENPs and Omnipaque, respectively. The red and yellow arrowheads indicate the heart and bladder area, respectively. (c) shows the corresponding CT value of heart and bladder at different time points post injection.

Cytocompatibility is a key issue for a material to be used in biomedical applications.[7, 24] We next explored the cytocompatibility of the PEGylated Au DENPs *via* MTT cell viability assay (Figure S5, ESI†). It can be seen that the formed $\{(Au^0)_8$-G2-*m*PEG$\}$ DENPs do not display apparent cytotoxicity in the concentration ranging from 0 to 3000 nM when compared with the PBS control. This demonstrates that the PEGylated Au DENPs possess desirable cytocompatibility.

The cytocompatibility of $\{(Au^0)_8$-G2-*m*PEG$\}$ DENPs was further confirmed by phase contrast microscopic visualization of the morphology of KB cells treated with the particles for 24 h (Figure S6, ESI†). It is clear that after treated with the PEGylated Au DENPs with a concentration range of 1000-3000 nM, the cells are pretty healthy, similar to the control cells treated with PBS. These cell morphology observation results validate the MTT assay data.

The X-ray attenuation property of the formed $\{(Au^0)_8$-G2-*m*PEG$\}$ DENPs was investigated in comparison with a conventional iodine-based small molecular CT contrast agent, Omnipaque (Figure S7, ESI†). CT phantom images of the aqueous suspensions of PEGylated Au DENPs reveal that the brightness of the CT image increases with the particle concentration, similar to Omnipaque (Figure S7a, ESI†), and the CT image of PEGylated Au DENPs is much brighter than that of Omnipaque at the concentration of Au or iodine above 0.04 M.

Further quantitative analysis data reveal that with the increase of the molar concentration of active element (Au or iodine), the X-ray attenuation intensity of both $\{(Au^0)_8$-G2-*m*PEG$\}$ DENPs and Omnipaque increases (Figure S7b, ESI†). Under similar concentrations of radiodense element, the $\{(Au^0)_8$-G2-*m*PEG$\}$ DENPs show much higher CT values than Omnipaque, in agreement with our previous work.[41, 42] The better X-ray attenuation property of Au DENPs than that of Omnipaque may render them with improved CT imaging sensitivity.

We next explored the *in vivo* CT imaging performance of the PEGylated Au DENPs. After intravenous injection of the particles, CT images of heart and bladder (Figure 2) were collected. The bladder CT imaging was performed in order to compare the excretion behavior of the Au DENPs with that of Omnipaque. It is clear that at 15-90 min post injection of the particles, the CT images of heart are much brighter than those of the Omnipaque group (Figure 2a), and the brightness of the heart starts to decay after 15 min for both Au DENPs and Omnipaque. In contrast, the brightness of the CT images of the bladder for the Omnipaque group is much higher than that for the Au DENP group (Figure 2b) at 15-90 min post injection, indicating a much faster metabolism process of Omnipaque. Our results suggest that the injection of PEGylated Au DENPs may enable a better CT imaging of mouse heart than Omnipaque due to the prolonged blood circulation time of the particles.

The better CT imaging performance of Au DENPs was further confirmed by quantitative measurement of the CT values of the mouse heart and bladder (Figure 2c). It can be clearly seen that the CT value of heart for the Au DENP group is obviously much higher than that for the Omnipaque control at 15-90 min post injection, indicating that the PEGylated Au DENPs enable an enhanced CT imaging of the heart. Although the CT values of the heart using the Au DENPs are improved in a range of 36.5-64.2% at the studied corresponding time points (15-90 min) when compared to those using Omnipaque, further improvement of heart CT imaging may be achievable after surface modification of Au DENPs with appropriate targeting ligands. The decayed CT value with time post injection for both groups is attributed to the metabolism process of the contrast agents. For the case of bladder imaging, the CT value of the bladder for the Omnipaque group reaches approximately 1500 HU at 15 min post injection and maintains high values till 90 min, indicating the fast metabolism process of the small molecular Omnipaque. In contrast, the metabolism process of Au DENPs is quite slow, and the bladder CT value for the Au DENP group increases gradually with the time post injection, and the CT value is less than 75 HU at 90 min post injection. Our results reveal that Omnipaque can be quickly excreted out of body through urinary system, while the PEGylated Au DENPs display a much slower metabolization, enabling effective CT imaging of heart.

It should be noted that the mice injected with the PEGylated

Au DENPs are pretty healthy after at least one month post injection, indicating the good biocompatibility of the particles. The Au biodistribution data show that only a small amount of Au still remains in the spleen, liver, and kidney after one week post injection (Figure S8, ESI†). This indicates that the PEGylated Au DENPs are able to be excreted out of the body with the time. Taken together, our results suggest that the PEGylated Au DENPs can be used as contrast agents for effective CT imaging of mouse heart due to the prolonged blood circulation time.

The enhanced CT imaging of mouse heart using PEGylated Au DENPs drove us to further pursue the applicability to use them for CT imaging of a tumor model *via* the known enhanced permeability and retention (EPR) effect.[48, 49] After administrating the PEGylated Au DENPs *via* either intraperitoneal or intravenous injection into the xenografted KB tumor-bearing mice, CT scanning of the mice was performed (Figure 3a). It can be seen that the tumor CT contrast enhancement is greater than that of the mice before injection with the time post injection for both injection routes. The tumor CT imaging enhancement was further quantified by measuring the tumor CT values at different time points post-injection (Figure 3b). For intraperitoneal injection group, the tumor CT value increases gradually after injection and shows significant difference at the studied time points compared to that before injection. The highest CT enhancement appears at 60 min post injection, followed by slight decrease of the CT value at 90 min post injection, which may be caused by the excretion of particles from the tumor tissue. In the case of intravenous injection, the tumor CT value is enhanced gradually till 90 min post-injection, which may be because the PEGylated Au DENPs can be continuously enriched in the tumor site through blood circulation. Our results suggest that PEGylated Au DENPs enable effective tumor CT imaging *via* EPR effect, similar to our previous result.[7] It seems that intravenous injection is more effective in enhanced tumor CT imaging than the intraperitoneal route.

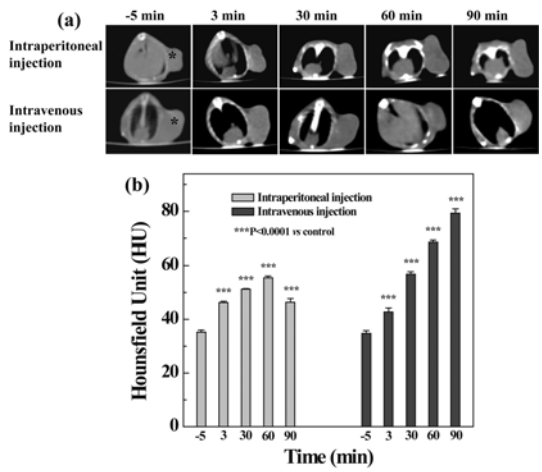

Figure 3. (a) CT images of a tumor model before and after intraperitoneal and intravenous injection of PEGylated Au DENPs, respectively. The stars indicate the tumor area. (b) shows the corresponding CT value of tumor area at different time points post injection.

To confirm the tumor uptake of PEGylated Au DENPs, the biodistribution of Au element in several major organs such as heart, liver, spleen, lung, kidney, and tumor was investigated by ICP-OES (Figure S9, ESI†). It can be clearly seen that besides kidney, the majority of the Au element is uptaken by spleen and lung at 90 min post-injection for both injection routes, which are associated with the reticuloendothelial system (RES).[50] This indicates that besides the tumor accumulation and renal metabolization, the PEGylated Au DENPs can be cleared mainly through the RES. It appears that the Au mass in these organs for the intraperitoneal injection group is much lower than that in the corresponding organs for the intravenous injection group, which is likely due to the fact that the intravenously injected Au DENPs experience a fast blood circulation, enabling a fast clearance of the particles by the RES. Overall, the Au uptake data suggest that the PEGylated Au DENPs can be uptaken by the tumor tissue *via* two different administration routes, allowing for effective tumor CT imaging.

Conclusions

In summary, we develop a robust approach to fabricating PEGylated Au DENPs for CT imaging applications using low generation dendrimers. Our results suggest that PEGylation modification of G2 PAMAM dendrimers is able to significantly enlarge the dendrimer periphery and geometry, allowing for effective entrapment of AuNPs within the dendrimer interiors. The formed PEGylated Au DENPs with good stability and cytocompatibility in the given concentration range display much stronger X-ray attenuation intensity than the clinically used CT contrast agent, Omnipaque at the same concentration of radiodense element (Au or iodine). These properties of the formed particles enable enhanced CT imaging of mouse heart and CT imaging of a xenografted tumor model *in vivo*. With the versatile dendrimer surface modification chemistry, multifunctional PEGylated Au DENPs may be formed using cost effective low-generation PAMAM dendrimers, thereby providing an effective platform for CT imaging of different biological systems.

This research is financially supported by the National Natural Science Foundation of China (21273032, 81341050, 81101150, and 81270032), and the Fund of the Science and Technology Commission of Shanghai Municipality (11nm0506400 for X. S., 12520705500 for M. S., and 11JC1410500 for G. Z.), the Program for Professor of Special Appointment (Eastern Scholar) at Shanghai Institutions of Higher Learning, and the Fundamental Research Funds for the Central Universities (for M. S. and X. S.). X. S. gratefully acknowledges the Fundação para a Ciência e a Tecnologia (FCT) and Santander bank for the Invited Chair in Nanotechnology, and the FCT for funding through the project PTDC/CTM-NAN/1748/2012.

Notes and references

[a] *State Key Laboratory for Modification of Chemical Fibers and Polymer Materials, Donghua University, Shanghai 201620, People's Republic of China.*
[b] *College of Chemistry, Chemical Engineering and Biotechnology, Donghua University, Shanghai 201620, People's Republic of China. Email: xshi@dhu.edu.cn*
[c] *Department of Radiology, Shanghai First People's Hospital, School of Medicine, Shanghai Jiaotong University, 100 Haining Road, Shanghai 200080, People's Republic of China. Email: guixiangzhang@sina.com*

[d] *CQM- Centro de Química da Madeira, Universidade da Madeira, Campus da Penteada, 9000-390 Funchal, Portugal*

† Electronic Supplementary Information (ESI) available: [Experimental protocols; detail characterization data; stability and cytocompatibility test results; *in vivo* distribution data]. See DOI: 10.1039/b000000x/

‡ These authors equally contributed to this work.

1. N. Lee, S. H. Choi and T. Hyeon, *Adv. Mater.*, 2013, **25**, 2641-2660.
2. H. Lusic and M. W. Grinstaff, *Chem. Rev.*, 2011, **113**, 1641-1666.
3. K. E. deKrafft, Z. Xie, G. Cao, S. Tran, L. Ma, O. Z. Zhou and W. Lin, *Angew. Chem.-Int. Edit.*, 2009, **121**, 10085-10088.
4. F. Hyafil, J. C. Cornily, J. E. Feig, R. Gordon, E. Vucic, V. Amirbekian, E. A. Fisher, V. Fuster, L. J. Feldman and Z. A. Fayad, *Nat. Med.* , 2007, **13**, 636-641.
5. Y. Liu, K. Ai, J. Liu, Q. Yuan, Y. He and L. Lu, *Angew. Chem.-Int. Edit.*, 2012, **51**, 1437-1442.
6. H. Liu, M. W. Shen, J. L. Zhao, J. Y. Zhu, T. T. Xiao, X. Y. Cao, G. X. Zhang and X. Shi, *Analyst*, 2013.
7. H. Wang, L. F. Zheng, C. Peng, R. Guo, M. W. Shen, X. Shi and G. X. Zhang, *Biomaterials*, 2011, **32**, 2979-2988.
8. C. Haller and I. Hizoh, *Invest. Radiol.*, 2004, **39**, 149-154.
9. I. Hizoh and C. Haller, *Invest. Radiol.*, 2002, **37**, 428-434.
10. A. Jakhmola, N. Anton and T. F. Vandamme, *Adv. Healthcare Mater.*, 2012, **1**, 413-431.
11. M. Shilo, T. Reuveni, M. Motiei and R. Popovtzer, *Nanomedicine*, 2012, **7**, 257-269.
12. K. Ai, Y. Liu, J. Liu, Q. Yuan, Y. He and L. Lu, *Adv. Mater.*, 2011, **23**, 4886-4891.
13. Y. Fang, C. Peng, R. Guo, L. F. Zheng, J. B. Qin, B. Q. Zhou, M. W. Shen, X. W. Lu, G. X. Zhang and X. Shi, *Analyst*, 2013, **138**, 3172-3180.
14. O. Rabin, J. M. Perez, J. Grimm, G. Wojtkiewicz and R. Weissleder, *Nat. Mater.*, 2006, **5**, 118-122.
15. Z. Liu, F. Pu, J. H. Liu, L. Y. Jiang, Q. H. Yuan, Z. Q. Li, J. S. Ren and X. G. Qu, *Nanoscale*, 2013, **5**, 4252-4261.
16. R. Guo, H. Wang, C. Peng, M. W. Shen, L. F. Zheng, G. X. Zhang and X. Shi, *J. Mater. Chem.*, 2011, **21**, 5120-5127.
17. I.-C. Sun, D.-K. Eun, J. H. Na, S. Lee, I.-J. Kim, I.-C. Youn, C.-Y. Ko, H.-S. Kim, D. Lim and K. Choi, *Chem. Eur. J.*, 2009, **15**, 13341-13347.
18. H. Wang, L. F. Zheng, C. Peng, M. W. Shen, X. Shi and G. X. Zhang, *Biomaterials*, 2013, **34**, 470-480.
19. S.-W. Chou, Y.-H. Shau, P.-C. Wu, Y.-S. Yang, D.-B. Shieh and C.-C. Chen, *J. Am. Chem. Soc.*, 2010, **132**, 13270-13278.
20. M. W. Galper, M. T. Saung, V. Fuster, E. Roessl, A. Thran, R. Proksa, Z. A. Fayad and D. P. Cormode, *Invest. Radiol.*, 2012, **47**, 475-481.
21. J. F. Hainfeld, D. N. Slatkin, T. M. Focella and H. M. Smilowitz, *Br. J. Radiol.*, 2006, **79**, 248-253.
22. D. Kim, S. Park, J. H. Lee, Y. Y. Jeong and S. Jon, *J. Am. Chem. Soc.*, 2007, **129**, 7661-7665.
23. H. Liu, Y. H. Xu, S. H. Wen, Q. Chen, L. F. Zheng, M. W. Shen, J. L. Zhao, G. X. Zhang and X. Shi, *Chem. Eur. J.*, 2013, **19**, 6409-6416.
24. H. Liu, Y. H. Xu, S. H. Wen, J. Y. Zhu, L. F. Zheng, M. W. Shen, J. L. Zhao, G. X. Zhang and X. Shi, *Polym. Chem.*, 2013, **4**, 1788-1795.
25. E. Boisselier, A. K. Diallo, L. Salmon, C. Ornelas, J. Ruiz and D. Astruc, *J. Am. Chem. Soc.*, 2010, **132**, 2729-2742.
26. L. W. Hoffman, G. G. Andersson, A. Sharma, S. R. Clarke and N. H. Voelcker, *Langmuir*, 2011, **27**, 6759-6767.
27. R. Guo, H. Wang, C. Peng, M. W. Shen, M. J. Pan, X. Y. Cao, G. X. Zhang and X. Shi, *J. Phys. Chem. C*, 2009, **114**, 50-56.
28. X. Shi, I. Lee and J. R. Baker, Jr., *J. Mater. Chem.*, 2008, **18**, 586-593.
29. X. Shi, S. H. Wang, S. Meshinchi, M. E. Van Antwerp, X. Bi, I. Lee and J. R. Baker, Jr., *Small*, 2007, **3**, 1245-1252.
30. R. Guo and X. Shi, *Curr. Drug Metab.*, 2012, **13**, 1097-1109.
31. M. Shen and X. Shi, *Nanoscale*, 2010, **2**, 1027-1032.
32. D. A. Tomalia and J. M. J. Frechet, eds., *Dendrimers and Other Dendritic Polymers*, John Wiley & Sons Ltd, New York, 2001.
33. Q. Chen, K. A. Li, S. H. Wen, H. Liu, C. Peng, H. D. Cai, M. W. Shen, G. X. Zhang and X. Shi, *Biomaterials*, 2013, **34**, 5200-5209.
34. S. H. Wen, K. A. Li, H. D. Cai, Q. Chen, M. W. Shen, Y. P. Huang, C. Peng, W. X. Hou, M. F. Zhu, G. X. Zhang and X. Shi, *Biomaterials*, 2013, **34**, 1570-1580.
35. X. Shi, S. H. Wang, H. Sun and J. R. Baker, Jr., *Soft Matter*, 2007, **3**, 71-74.
36. X. Shi, T. R. Ganser, K. Sun, L. P. Balogh and J. R. Baker, Jr., *Nanotechnology*, 2006, **17**, 1072-1078.
37. X. Shi, S. H. Wang, M. E. Van Antwerp, X. Chen and J. R. Baker, Jr., *Analyst*, 2009, **134**, 1373-1379.
38. C. Peng, K. A. Li, X. Y. Cao, T. T. Xiao, W. X. Hou, L. F. Zheng, R. Guo, M. W. Shen, G. X. Zhang and X. Shi, *Nanoscale*, 2012, **4**, 6768-6778.
39. T. T. Xiao, S. H. Wen, H. Wang, H. Liu, M. W. Shen, J. L. Zhao, G. X. Zhang and X. Shi, *J. Mater. Chem. B*, 2013, **1**, 2773-2780.
40. H. Liu, M. W. Shen, J. L. Zhao, R. Guo, X. Y. Cao, G. X. Zhang and X. Shi, *Colloid Surf. B-Biointerfaces*, 2012, **94**, 58-67.
41. C. Peng, L. F. Zheng, Q. Chen, M. W. Shen, R. Guo, H. Wang, X. Y. Cao, G. X. Zhang and X. Shi, *Biomaterials*, 2012, **33**, 1107-1119.
42. C. Peng, J. B. Qin, B. Q. Zhou, Q. Chen, M. W. Shen, M. F. Zhu, X. W. Lu and X. Shi, *Polym. Chem.*, 2013, **4**, 4412-4424.
43. Q.-Y. Cai, S. H. Kim, K. S. Choi, S. Y. Kim, S. J. Byun, K. W. Kim, S. H. Park, S. K. Juhng and K.-H. Yoon, *Invest. Radiol.*, 2007, **42**, 797-806.
44. C. Kojima, Y. Umeda, M. Ogawa, A. Harada, Y. Magata and K. Kono, *Nanotechnology*, 2010, **21**, 245104.
45. S. D. Brown, P. Nativo, J.-A. Smith, D. Stirling, P. R. Edwards, B. Venugopal, D. J. Flint, J. A. Plumb, D. Graham and N. J. Wheate, *J. Am. Chem. Soc.*, 2010, **132**, 4678-4684.
46. K. Esumi, A. Suzuki, A. Yamahira and K. Torigoe, *Langmuir*, 2000, **16**, 2604-2608.
47. G. M. Pavan, A. Barducci, L. Albertazzi and M. Parrinello, *Soft Matter*, 2013, **9**, 2593-2597.
48. A. K. Iyer, G. Khaled, J. Fang and H. Maeda, *Drug Discov. Today*, 2006, **11**, 812-818.
49. H. Maeda, J. Wu, T. Sawa, Y. Matsumura and K. Hori, *J. Control. Release*, 2000, **65**, 271-284.
50. J.-W. Yoo, E. Chambers and S. Mitragotri, *Curr. Pharm. Design*, 2010, **16**, 2298-2307.